

Chiral superconductivity in nematic states

Shuhei Takamatsu^{1,*} and Youichi Yanase²

¹*Graduate School of Science and Technology, Niigata University, Niigata, 950-2181, Japan.*

²*Department of Physics, Niigata University, Niigata, 950-2181, Japan.*

(Dated: August 18, 2018)

We investigate chiral superconductivity which occurs in the electronic nematic state. A vortex state in a c -axis magnetic field is studied on the basis of the two-component Ginzburg-Landau model for nematic-chiral superconductors. It is shown that various vortex lattice structures are stabilized by nontrivial cooperation of nematicity and chirality in superconductors. In particular, the vortex lattice structural transition occurs when a square anisotropy parameter ν is positive (negative) and the nematicity is induced along the $[110]$ axis ($[100]$ axis). We discuss nematic-chiral superconductivity in URu_2Si_2 , Sr_2RuO_4 , and UPt_3 . An experimental test for the examination of nematic order and chiral superconductivity is proposed.

PACS numbers: 74.20.De, 74.25.Uv, 74.70.Tx, 74.70.Pq

I. INTRODUCTION

Recent studies on the strongly correlated electron systems have explored the chiral superconductivity with broken time-reversal symmetry. A chiral $(p_x \pm ip_y)$ -wave superconductivity analogous to the ^3He A phase has been established in Sr_2RuO_4 ^{1,2}, and a chiral $(d_{zx} \pm id_{yz})$ -wave superconductivity in URu_2Si_2 has been identified by recent experimental studies³⁻⁷. Spontaneous time-reversal symmetry breaking characteristic of chiral superconductors has been observed in both compounds^{5,6,8,9}. Furthermore, a recent polar Kerr rotation measurement detected broken time-reversal symmetry in UPt_3 ¹⁰, and thus a chiral superconducting (SC) state which belongs to the E_{1u} , E_{2u} , or E_{1g} representation is suggested.

Interestingly, chiral superconductivity coexists with a nematic order in at least some of these superconductors. Nematic states in itinerant electron systems analogous to classical liquid crystals have been one of the highlights in recent condensed-matter physics¹¹. A "quantum nematic liquid crystal" accompanying spontaneous rotation symmetry breaking has been studied in some strongly correlated electron systems. For instance, a nematic order arising from the fluctuating stripe order has been proposed for cuprate superconductors¹², and a nematic state in a bilayer ruthenate $\text{Sr}_3\text{Ru}_2\text{O}_7$ has been investigated extensively¹³. Furthermore, a nematic fluctuation in Fe-based superconductors has been investigated^{14,15} and identified as a possible glue of Cooper pairs^{16,17}.

There is accumulating evidence for a nematic order in the so-called hidden-ordered state of URu_2Si_2 ¹⁸. The magnetic torque¹⁹, cyclotron resonance²⁰, NMR²¹, and x-ray scattering²² measurements uncovered a broken fourfold rotation symmetry below the hidden-order temperature $T < T_{\text{HO}}$, although another NMR measurement did not detect any broken symmetry²³. Since the SC transition is a continuous second-order phase transition, the nematic order has to coexist with the superconductivity below T_c . Indeed, a signature of nematic order has been observed in the SC state²⁴. A kink in the lower critical field H_{c1} has been attributed to a second SC tran-

sition due to the broken fourfold rotation symmetry. It is also known from early experimental results^{25,26} that the sixfold rotation symmetry in the hexagonal crystal lattice of UPt_3 is broken in the SC state. The splitting of two transition temperatures and the existence of the A phase at zero magnetic field has been attributed to the effect of a nematicity^{27,28}. Although the origin of broken rotation symmetry is still unclear, the antiferromagnetic order^{26,29} may cause the nematicity. What is clear is that a nematicity plays an essential role in the multiple SC phases in UPt_3 . Although a spontaneous nematic order does not occur in Sr_2RuO_4 , a nematicity is artificially induced by uniaxial pressure. Indeed, an enhancement of the transition temperature due to the uniaxial pressure has been observed in Sr_2RuO_4 ³⁰. Thus, all the chiral superconductors known up to now coexist with the nematicity.

It is interesting to study the vortex state of these nematic-chiral superconductors because of the following two reasons. First, an effect of nematic order competes with the gradient mixing in order parameters due to a magnetic field. Although the nematicity favors a nonchiral state, such as the $(p_x \pm p_y)$ -wave state or $(d_{zx} \pm d_{yz})$ -wave state, the magnetic field along the c axis stabilizes the chiral state, such as the $(p_x \pm ip_y)$ -wave state or $(d_{zx} \pm id_{yz})$ -wave state, through the gradient mixing. Therefore, the order parameter in nematic-chiral superconductors is nontrivial. Second, various vortex lattice structures are stabilized in the chiral superconductors because of the gradient coupling of two-component order parameters³¹⁻³³. Thus, it is expected that rich vortex lattice phases appear in nematic-chiral superconductors. From the other perspective, the vortex state in chiral superconductors is sensitive to the nematicity in the underlying electronic state. Therefore, the vortex lattice structure will be a sensitive probe for detecting the nematic order.

In this paper we investigate the vortex state of nematic-chiral superconductors on the basis of the Ginzburg-Landau (GL) theory. Signatures of the nematic order in the chiral SC state are clarified. The or-

ganization of this paper is as follows. In Sec. II, we introduce the GL model and describe a variational method by which we study the vortex state. In Sec. III, we show the phase diagram for the order parameter and vortex lattice structure. Experimental results on URu₂Si₂, Sr₂RuO₄, and UPt₃ are discussed and future experimental studies are proposed in Sec. IV.

II. GINZBURG-LANDAU THEORY

A. Ginzburg-Landau model

In this section, we construct a two-component Ginzburg-Landau (GL) model for chiral superconductors in the nematic state. Essential variables are two-component order parameters, $(\eta_a(\mathbf{r}), \eta_b(\mathbf{r}))$, by which the pairing function is described as $\Delta(\mathbf{r}, \mathbf{k}) = \eta_a(\mathbf{r})\phi_a(\mathbf{k}) + \eta_b(\mathbf{r})\phi_b(\mathbf{k})$. Here, $\phi_a(\mathbf{k})$ and $\phi_b(\mathbf{k})$ stand for pairing functions in the momentum space which belong to a two-dimensional representation of the crystal point group³⁴. For instance, the chiral $(p_x \pm ip_y)$ -wave SC state in Sr₂RuO₄ belongs to the E_u representation of the D_{4h} point group³⁵, while the chiral $(d_{zx} \pm id_{yz})$ -wave state in URu₂Si₂ belongs to the E_g representation. The chiral f -wave superconductivity, which belongs to the E_{2u} representation of the D_{6h} point group, has been suggested for a representative multicomponent superconductor UPt₃²⁷. On the other hand, a recent thermal conductivity measurement indicated the E_{1u} representation³⁶. All of these chiral SC states are represented by two-component order parameters $(\eta_a(\mathbf{r}), \eta_b(\mathbf{r}))$ as above, although the pairing functions $\phi_a(\mathbf{k})$ and $\phi_b(\mathbf{k})$ depend on materials.

First, we discuss a GL model in the absence of the nematicity. Assuming a weak nematicity, we later add a quadratic symmetry-breaking term. The symmetric part of the GL free-energy density has been obtained as

$$\begin{aligned}
F_0 = & \alpha(|\eta_a|^2 + |\eta_b|^2) + \frac{\beta_1}{2}(|\eta_a|^2 + |\eta_b|^2)^2 \\
& + \frac{\beta_2}{2}(\eta_a\eta_b^* - \text{c.c.})^2 + \beta_3|\eta_a|^2|\eta_b|^2 \\
& + \kappa_1(|D'_x\eta_a|^2 + |D'_y\eta_b|^2) \\
& + \kappa_2(|D'_x\eta_b|^2 + |D'_y\eta_a|^2) \\
& + \kappa_3[(D'_x\eta_a)(D'_y\eta_b)^* + \text{c.c.}] \\
& + \kappa_4[(D'_x\eta_b)(D'_y\eta_a)^* + \text{c.c.}]
\end{aligned} \tag{1}$$

for chiral superconductors in the type-II limit³⁴. Following the conventional notation, we denote $\alpha = \alpha_0(T/T_c^0 - 1)$, with T_c^0 being the transition temperature at zero magnetic field, and covariant derivatives $D'_j = -i\partial_j + (2\pi/\Phi_0)A_j$, with $\Phi_0 = hc/2|e|$. We omit gradient terms containing z derivatives because we focus on the vortex state in magnetic fields applied along the c axis.

In the weak-coupling BCS theory, parameters are given by the following relations: $\beta_2/\beta_1 = \langle \phi_a^2 \phi_b^2 \rangle_{\text{FS}} / \langle \phi_a^4 \rangle_{\text{FS}}$,

$\beta_3/\beta_1 = 3\beta_2/\beta_1 - 1$, $\kappa_2/\kappa_1 = \langle \phi_a^2 v_y^2 \rangle_{\text{FS}} / \langle \phi_a^2 v_x^2 \rangle_{\text{FS}}$, and $\kappa_3/\kappa_1 = \kappa_4/\kappa_1 = \langle \phi_a \phi_b v_x v_y \rangle_{\text{FS}} / \langle \phi_a^2 v_x^2 \rangle_{\text{FS}}$, where v_x and v_y are Fermi velocities in the ab plane and brackets $\langle \dots \rangle_{\text{FS}}$ denote an average over the Fermi surface. Despite three independent parameters, β_2/β_1 , κ_2/κ_1 , and κ_3/κ_1 , a single-parameter description of the GL model has been adopted in studies of chiral $(p_x \pm ip_y)$ -wave superconductivity^{31–33}. As shown by Agterberg^{31,32}, the coupling constants are represented by a single-parameter ν as³⁷

$$\beta_2/\beta_1 = \kappa_2/\kappa_1 = \kappa_3/\kappa_1 = (1 + \nu)/(3 - \nu) \tag{2}$$

when we assume pairing functions $(\phi_a(\mathbf{k}), \phi_b(\mathbf{k})) = (v_x(\mathbf{k}), v_y(\mathbf{k}))$ (Agterberg model). Adopting similar pairing functions for the chiral $(d_{zx} \pm id_{yz})$ -wave SC state, $(\phi_a(\mathbf{k}), \phi_b(\mathbf{k})) = (v_x(\mathbf{k})f(k_z), v_y(\mathbf{k})f(k_z))$, with $f(k_z)$ being an odd function (extended Agterberg model), we approximately obtain parameters shown in Eq. (2). Strictly speaking, the single-parameter description breaks down since $\beta_2/\beta_1 \neq \kappa_2/\kappa_1 = \kappa_3/\kappa_1$. However, the deviation is negligible, $\beta_2/\beta_1 - \kappa_2/\kappa_1 \ll 1$, for a smooth function $f(k_z)$. Thus, the single-parameter description is also applicable to the chiral $(d_{zx} \pm id_{yz})$ -wave superconductors. In crystals satisfying the D_{4h} point group, the parameter ν indicates the square anisotropy in the Fermi surface, because $\nu = 0$ for the cylindrical or spherical Fermi surface, while $\nu \neq 0$ otherwise. On the other hand, the chiral E_{1u} state in the D_{6h} point-group symmetry is similarly described as $(\phi_a(\mathbf{k}), \phi_b(\mathbf{k})) = (v_x(\mathbf{k})f(k_z), v_y(\mathbf{k})f(k_z))$ with $f(k_z)$ being an even function. Then, we obtain $\beta_2/\beta_1 = \kappa_2/\kappa_1 = \kappa_3/\kappa_1 = 1/3$, and thus, $\nu = 0$ in Eq. (2) irrespective of the Fermi surface³⁸. Thus, we can rely on the single-parameter description of the GL model for these chiral p -wave, d -wave, and f -wave superconductivities when the Fermi velocity and pairing functions have a smooth momentum dependence. Adopting the single-parameter description, we investigate the vortex state in chiral superconductors. On the other hand, Eq. (2) seriously breaks down in the chiral E_{2u} state in the D_{6h} point-group symmetry. Thus, the chiral E_{2u} state is beyond the scope of our study, but we will briefly discuss it in Sec. IV.

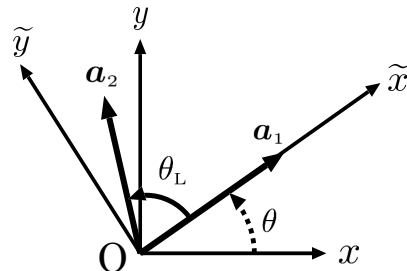


FIG. 1. Primitive vectors of the vortex lattice \mathbf{a}_1 and \mathbf{a}_2 . Two-dimensional coordinates (x, y) and (\tilde{x}, \tilde{y}) and angles θ_L and θ are illustrated.

We rewrite the GL model using order parameters in the chirality basis, $\eta_1 = \gamma(\eta_a - i\eta_b)/\sqrt{2}$ and $\eta_2 = \gamma(\eta_a +$

$i\eta_b)/\sqrt{2}$ with, $\gamma = (\tilde{\beta}_1/\alpha_0)^{1/2}$ and $\tilde{\beta}_1 = \beta_1 - \beta_2 + \beta_3/2 = 2\beta_1/(3 - \nu)$. With the two-dimensional coordinate rotated through an angle θ around the z axis (see Fig. 1), the dimensionless free-energy density is given by

$$\begin{aligned}
f_0 = & \frac{T - T_c^0}{T_c^0} (|\eta_1|^2 + |\eta_2|^2) + \frac{1}{2} (|\eta_1|^4 + |\eta_2|^4) \\
& + 2|\eta_1|^2|\eta_2|^2 - \frac{\nu}{2} [(\eta_1\eta_2^*)^2 + \text{c.c.}] \\
& + |D_{\bar{x}}\eta_1|^2 + |D_{\bar{y}}\eta_1|^2 + |D_{\bar{x}}\eta_2|^2 + |D_{\bar{y}}\eta_2|^2 \\
& + \frac{1}{2} \{ (e^{2i\theta} - \nu e^{-2i\theta}) \\
& \times [(D_{\bar{x}}\eta_1)(D_{\bar{x}}\eta_2)^* - (D_{\bar{y}}\eta_1)(D_{\bar{y}}\eta_2)^*] + \text{c.c.} \} \\
& + \frac{1}{2} \{ i(e^{2i\theta} + \nu e^{-2i\theta}) \\
& \times [(D_{\bar{x}}\eta_1)(D_{\bar{y}}\eta_2)^* + (D_{\bar{y}}\eta_1)(D_{\bar{x}}\eta_2)^*] + \text{c.c.} \}, \quad (3)
\end{aligned}$$

where the unit of energy, length, and magnetic field are $\alpha_0^2/\tilde{\beta}_1$, $\xi = [(\kappa_1 + \kappa_2)/2\alpha_0]^{1/2}$, and $\Phi_0/2\pi\xi^2$, respectively. The covariant derivatives are denoted as $D_{\bar{j}} = -i\partial_{\bar{j}} + A_{\bar{j}}$. We focus on the magnetic field along the c axis, and choose the vector potential $\mathbf{A} = -\tilde{y}H\mathbf{e}_{\bar{x}}$. In the reasonable parameter range $|\nu| \leq 1$, a chiral SC state with $(\eta_1, \eta_2) \propto (1, 0)$ or $(\eta_1, \eta_2) \propto (0, 1)$ is stable at zero magnetic field.

A weak nematicity leading to the violation of fourfold or sixfold rotational symmetry is taken into account by adding the symmetry-breaking term in the quadratic form

$$f_{2h} = g(i\eta_1\eta_2^* + \text{c.c.}) = g\gamma^2(\eta_a\eta_b^* + \text{c.c.}) \quad (4)$$

to f_0 . Thus, the total free-energy density is given by

$$f = f_0 + f_{2h}. \quad (5)$$

The coupling constant g represents a lifting of degeneracy between two orbital pairing functions $\phi_a(\mathbf{k})$ and $\phi_b(\mathbf{k})$ due to the nematic order. As a consequence of the symmetry-breaking term, double SC transitions occur at zero magnetic field. In the high-temperature phase near the SC transition temperature, $T_{c2} < T < T_c$, a nonchiral state where $(\eta_1, \eta_2) \propto (1, \pm i)$ is stabilized, while a chiral state is stabilized below T_{c2} . The time-reversal symmetry is spontaneously broken in the low-temperature phase. The double SC transition has been observed in UPt_3 ²⁵⁻²⁸, and a signature of double SC transition has been reported in URu_2Si_2 ²⁴.

In Eq. (4) we assume a nematicity along the [110] direction to be consistent with experimental observations in URu_2Si_2 ¹⁹⁻²². The nematicity along the [100] axis is also investigated on the basis of our model. When we change the coordinate $\theta \rightarrow \theta + \pi/4$ and take the phase factor $(\eta_1, \eta_2) \rightarrow (\eta_1 e^{-i\pi/4}, \eta_2 e^{i\pi/4})$, the f_0 term is almost invariant except for the sign reversal $\nu \rightarrow -\nu$. Then, the symmetry-breaking term changes to

$$f'_{2h} = g(\eta_1\eta_2^* + \text{c.c.}) = g\gamma^2 (|\eta_a|^2 - |\eta_b|^2), \quad (6)$$

which is nothing but the symmetry-breaking term due to the nematicity along the [100] axis. A symmetry-breaking term of this form has been adopted for studies on multiple SC phases in UPt_3 ^{27,28}. We change the sign of ν instead of considering the symmetry-breaking term in Eq. (6) for studies of nematicity along the [100] axis.

B. Variational method

We investigate the order parameters and vortex lattice structure using the variational method. We assume variational wave functions of Cooper pairs so that the solution of the linearized GL equation is reproduced. First, we solve the linearized GL equation using the Landau-level expansion. Differentiating the quadratic terms in the f_0 term [Eq. (3)] with respect to η_1 and η_2 , we obtain the linearized GL equation in the absence of the symmetry-breaking term,

$$\begin{aligned}
\lambda \begin{pmatrix} \eta_1 \\ \eta_2 \end{pmatrix} = & \frac{1}{l_c^2} \begin{pmatrix} 1 + 2\Pi_+\Pi_- & e^{-2i\theta}\Pi_-^2 - \nu e^{2i\theta}\Pi_+^2 \\ e^{2i\theta}\Pi_+^2 - \nu e^{-2i\theta}\Pi_-^2 & 1 + 2\Pi_+\Pi_- \end{pmatrix} \\
& \times \begin{pmatrix} \eta_1 \\ \eta_2 \end{pmatrix}, \quad (7)
\end{aligned}$$

where $l_c = 1/\sqrt{H}$ and $\Pi_{\pm} = -(l_c/\sqrt{2})(D_{\bar{x}} \pm iD_{\bar{y}})$. The solution for the minimum eigenvalue $\lambda = \lambda_{\min}$ is represented as

$$\begin{pmatrix} \psi_{1+}(\mathbf{r}) \\ \psi_{2+}(\mathbf{r}) \end{pmatrix} = \sum_{n \geq 0} \begin{pmatrix} a_{4n}(\theta)\varphi_{4n}(\mathbf{r}, \rho, \sigma) \\ a_{4n+2}(\theta)\varphi_{4n+2}(\mathbf{r}, \rho, \sigma) \end{pmatrix}, \quad (8)$$

where $\varphi_n(\mathbf{r}, \rho, \sigma)$ denotes the n th Landau-level wave function. The leading term is the lowest Landau level of the positive chirality component, and thus, $(\psi_{1+}(\mathbf{r}), \psi_{2+}(\mathbf{r})) \simeq (a_0(\theta)\varphi_0(\mathbf{r}, \rho, \sigma), 0)$. We obtain another solution for the pairing state with a dominantly negative chirality,

$$\begin{pmatrix} \psi_{1-}(\mathbf{r}) \\ \psi_{2-}(\mathbf{r}) \end{pmatrix} = \sum_{n \geq 0} \begin{pmatrix} b_{4n+2}(\theta)\varphi_{4n+2}(\mathbf{r}, \rho, \sigma) \\ b_{4n}(\theta)\varphi_{4n}(\mathbf{r}, \rho, \sigma) \end{pmatrix}, \quad (9)$$

where the leading term is the lowest Landau level of the negative chirality component, $(\psi_{1-}(\mathbf{r}), \psi_{2-}(\mathbf{r})) \simeq (0, b_0(\theta)\varphi_0(\mathbf{r}, \rho, \sigma))$. Coefficients $a_n(\theta)$ and $b_n(\theta)$ are numerically determined. We assume variational wave functions consisting of a linear combination of the two solutions:

$$\begin{pmatrix} \eta_1(\mathbf{r}) \\ \eta_2(\mathbf{r}) \end{pmatrix} = C_+ \begin{pmatrix} \psi_{1+}(\mathbf{r}) \\ \psi_{2+}(\mathbf{r}) \end{pmatrix} + C_- \begin{pmatrix} \psi_{1-}(\mathbf{r}) \\ \psi_{2-}(\mathbf{r}) \end{pmatrix}, \quad (10)$$

where $|C_+|$ ($|C_-|$) represents the weight of Cooper pairs having dominantly positive (negative) chirality. The variational wave function is justified near the transition temperature and for a small symmetry-breaking term g , although the reconstruction of higher Landau levels affects the vortex lattice structure at low temperatures³³. Our

main result is concerned with the vortex lattice structural transition near T_c , and thus, the variational wave function is appropriate.

In order to study the vortex lattice structure, we adopt a general form of the n th Landau-level wave functions³⁹

$$\varphi_n(\mathbf{r}, \rho, \sigma) = \frac{1}{\sqrt{2^n \pi^{1/2} n!}} \sum_m c_m e^{2\pi i(m-1/2)\tilde{x}/a} \times H_n\left(\frac{\tilde{y}-y_m}{l_c}\right) e^{-(\tilde{y}-y_m)^2/2l_c^2}, \quad (11)$$

where $c_m = e^{i\pi m(\rho+1-m\rho)}$, $y_m = l_c \sqrt{2\pi\sigma}(m-1/2)$, and $H_n(y)$ is the Hermit polynomials. The vortex lattice structure is determined by the variables $\rho = (b/a) \cos \theta_L$ and $\sigma = (b/a) \sin \theta_L$. Primitive vectors are $\mathbf{a}_1 = a\mathbf{e}_{\tilde{x}}$ and $\mathbf{a}_2 = b(\cos \theta_L \mathbf{e}_{\tilde{x}} + \sin \theta_L \mathbf{e}_{\tilde{y}}) = a(\rho \mathbf{e}_{\tilde{x}} + \sigma \mathbf{e}_{\tilde{y}})$ (see Fig. 1). The area of the unit cell is $|\mathbf{a}_1 \times \mathbf{a}_2| = ab \sin \theta_L = 2\pi l_c^2$. The rectangular and centered rectangular lattices are formed for $\rho = 0$ and $\rho = 1/2$, respectively. The square and triangular lattices are special cases of them; $(\rho, \sigma) = (0, 1)$ or $(\rho, \sigma) = (1/2, 1/2)$ in the square lattice, and $(\rho, \sigma) = (1/2, \sqrt{3}/2)$ in the triangular lattice. The angle of a primitive vector \mathbf{a}_1 from the original x axis is θ , and it is dealt with as a variational parameter. Thus, variational parameters for the vortex lattice structure are ρ , σ , and θ .

Substituting Eqs. (8)-(11) into Eqs. (3) and (4) and integrating over the unit cell, we obtain the free-energy density as

$$F(C_+, C_-, \rho, \sigma, \theta) = \langle f \rangle_{\text{uc}} = \frac{1}{2\pi l_c^2} \int_{\text{uc}} f(\mathbf{r}) d^2 r. \quad (12)$$

The brackets $\langle \dots \rangle_{\text{uc}}$ denote an average over the unit cell. Optimizing variational parameters (C_+ , C_- , ρ , σ , θ) to minimize the free-energy density, we determine the order parameters and vortex lattice structure.

III. CHIRAL SUPERCONDUCTING STATES

A. Vortex lattice in the non-nematic state

In this section, we investigate the vortex state in the absence of nematicity. Thus, we consider a tetragonal or hexagonal system and choose the parameter $g = 0$. The effects of nematic order on the chiral SC state are studied in the following sections.

First, we determine the vortex lattice structure near the upper critical field. Since the symmetry-breaking term f_{2h} is absent, a solution of the linearized GL equation $(\eta_1, \eta_2) = C_+(\psi_{1+}(\mathbf{r}), \psi_{2+}(\mathbf{r}))$ minimizes the free energy near the SC transition. Thus, $C_- = 0$, and the vortex lattice structure is determined so as to minimize the Abrikosov parameter $\beta_A = 2 \langle f_4 \rangle_{\text{uc}} / (\langle |\psi_{1+}|^2 \rangle_{\text{uc}} + \langle |\psi_{2+}|^2 \rangle_{\text{uc}})^2$, where f_4 is the quartic term in Eq. (3). Figure 2 shows the Abrikosov parameter for various vortex

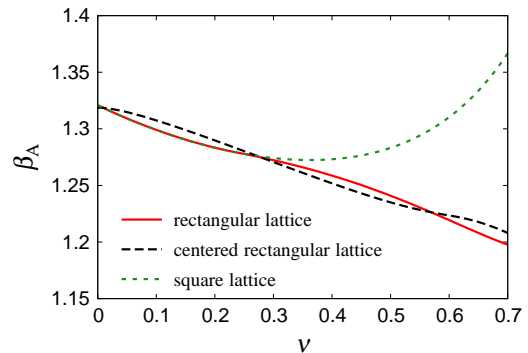


FIG. 2. (Color online) Abrikosov parameter β_A for the rectangular lattice ($\rho = 0$, red solid line) and centered rectangular lattice ($\rho = 1/2$, black long-dashed line) as a function of ν . The variational parameter σ is optimized to minimize β_A . The Abrikosov parameter for the square lattice $[(\rho, \sigma) = (0, 1)]$ is shown by the green short-dashed line. The other variational parameter θ is fixed to $\theta = 0$ ($\theta = \pi/4$) for $\nu > 0$ ($\nu < 0$), for which the Abrikosov parameter is optimized when $|\nu| > 0.0114$. When $|\nu| < 0.0114$, the optimized angle is $\theta = \pi/4$ ($\theta = 0$) for $\nu > 0$ ($\nu < 0$), but the θ dependence of β_A is negligible.

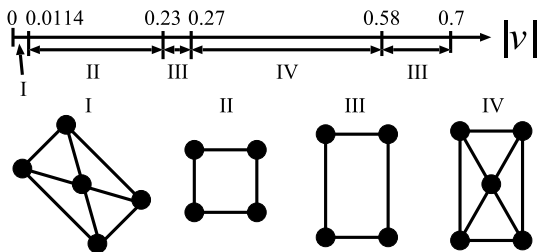


FIG. 3. Schematic of the vortex lattice structure near the upper critical field. We show the result for $\nu > 0$. The vortex lattice is rotated $\pi/4$ for $\nu < 0$.

lattice structures as a function of the anisotropy parameter ν , and we illustrate the vortex lattice structure which minimizes the free energy in Fig. 3. It is shown that the centered rectangular lattice, square lattice, rectangular lattice, and, again, centered rectangular lattice are stabilized with increasing $|\nu|$. These results are consistent with previous works which investigated the vortex lattice structure in the small- $|\nu|$ region³¹⁻³³. Agterberg showed that the square lattice is stable unless the anisotropy parameter is extraordinary small, $|\nu| < 0.0114$ ^{31,32}. The triangular lattice is formed at $\nu = 0$ like in conventional superconductors, and it is deformed with increasing $|\nu|$. The parameter σ decreases from $\sqrt{3}/2$ to $1/2$ when $|\nu|$ increases from 0 to 0.0114. The qualitatively same results have been obtained by Kita using a sophisticated calculation which takes into account higher Landau levels and screening current³³. He also found that the rectangular lattice is stabilized for a large anisotropy parameter $|\nu|$. Our calculation reproduces these results and, furthermore, shows that the centered rectangular lattice and

rectangular lattice are stabilized for $0.27 \leq |\nu| \leq 0.58$ and $0.58 \leq |\nu| \leq 0.7$, respectively. We do not consider a further large parameter $|\nu| > 0.7$ since the numerical convergence becomes worse.

Next, we show the phase diagram against magnetic fields and temperatures (H - T phase diagram) for two anisotropy parameters $\nu = 0.15$ and $\nu = 0.3$. For $\nu = 0.15$, the square vortex lattice is stable near the transition temperature $T = T_c(H)$, as illustrated in Fig. 3. Figure 4 shows that the structural transition occurs at a moderate temperature $T = T_{c2}(H)$, and the rectangular vortex lattice is stabilized below $T_{c2}(H)$. Figure 5 shows the magnetic field dependences of variational parameters $|C_{\pm}|$ and the "nematicity of the vortex lattice" b/a at $T/T_c^0 = 0.4$. It is shown that the emergence of nematicity $b/a - 1$ coincides with C_- , although $C_- = 0$ and $b/a = 1$ in the high magnetic field region, $H/H_{c2}(0) > 0.38$. Thus, the structural transition in the vortex lattice accompanies the mixing of chirality in the order parameter.

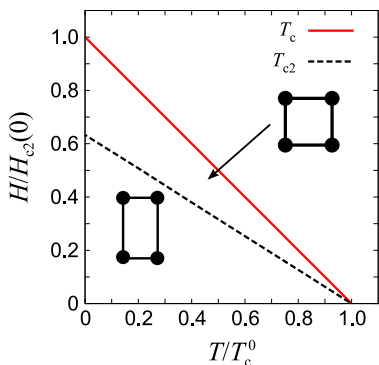


FIG. 4. (Color online) Phase diagram of the vortex lattice as a function of the dimensionless magnetic field $H/H_{c2}(0)$ and temperature T/T_c^0 for $(\nu, g) = (0.15, 0)$. The red solid line shows the SC transition temperature $T_c(H)$, while the black dashed line shows the second transition temperature $T_{c2}(H)$. The vortex lattice structures are shown schematically. The phase diagram is independent of the sign of ν , while the vortex lattice for $\nu < 0$ is rotated $\pi/4$ from that for $\nu > 0$.

On the other hand, the vortex lattice structural transition does not occur for $\nu = 0.3$. Then, the centered rectangular lattice is formed in the whole SC state (Fig. 6). Because of the orthorhombic symmetry of the vortex lattice, the order parameter for pairing with dominantly negative chirality is finite, $C_- \neq 0$. However, the positive chirality is favored by the linear coupling of magnetic field and chirality in Cooper pairs³¹, and therefore, $|C_+| \gg |C_-|$. A similar H - T phase diagram is obtained for the isotropic case $\nu = 0$. Then, the triangular vortex lattice is stabilized.

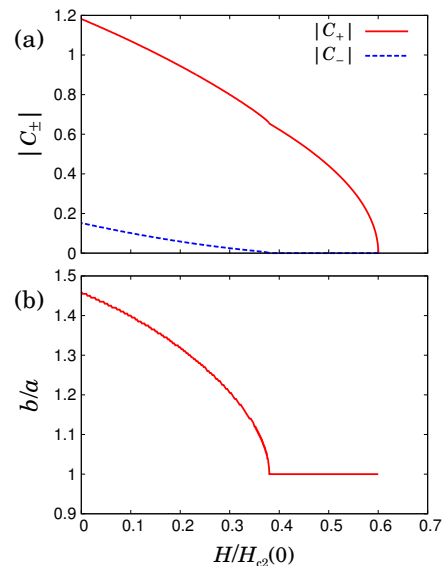


FIG. 5. (Color online) Magnetic field dependence of (a) order parameters $|C_{\pm}|$ and (b) a structural parameter $b/a (= \sigma)$ at $T/T_c^0 = 0.4$ for $(\nu, g) = (0.15, 0)$. The other structural parameters are $\theta_L = \pi/2$ ($\rho = 0$) and $\theta = 0$.

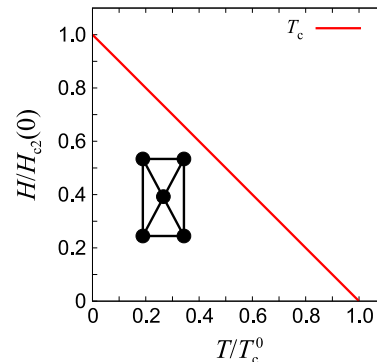


FIG. 6. (Color online) Phase diagram of the vortex lattice for $(\nu, g) = (0.3, 0)$. As shown schematically, the centered rectangular lattice is stabilized in the whole SC state.

B. Vortex lattice in the nematic state ($\nu > 0$)

Now we turn to the main topic of this paper. We study the vortex state of chiral superconductors which coexist with the nematic order. The GL model with a finite symmetry-breaking term ($g \neq 0$) is analyzed. The sign of the coupling constant g is not important at all, and thus, we assume $g > 0$. For $g < 0$, the vortex lattice rotates $\pi/2$. We choose $g = 0.05$ unless we explicitly state otherwise. The SC double transition occurs at zero magnetic field, and the splitting of two transition temperatures is 10% of T_c^0 for our choice of the coupling constant g . This splitting is consistent with the experimental data indicating a double transition in URu_2Si_2 ²⁴ and UPt_3 ²⁵⁻²⁸.

In a magnetic field $H > 0$, the chiral SC state with positive chirality $(\eta_1, \eta_2) \propto (1, 0)$ is favored by the gradient mixing in order parameters³¹. Then, the second SC transition is smeared and it changes to the chiral-nonchiral crossover (C-NC crossover in Figs. 7, 11, and 12). We show here that the vortex lattice structural transition occurs as a result of the C-NC crossover when the anisotropy parameter is positive, $\nu > 0$. Owing to the symmetry-breaking term, the phase diagram is no longer independent of the sign of ν . Thus, we study the case with $\nu > 0$ in this section, and the case with $\nu < 0$ is investigated in the next section. The isotropic case, $\nu = 0$, will be discussed for UPt_3 in Sec. IV.

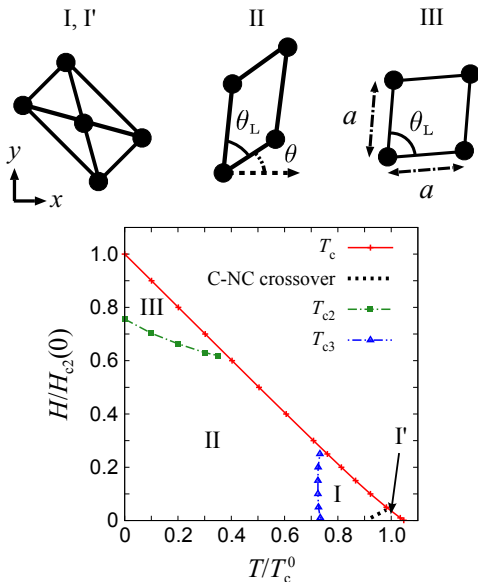


FIG. 7. (Color online) Phase diagram for $(\nu, g) = (0.15, 0.05)$. The red solid line shows the SC transition temperature $T_c(H)$. The green squares and blue triangles show the critical point of the vortex lattice structural transition. The black dotted line depicts the C-NC crossover, which we define by $|C_-| = 0.7|C_+|$. Phase I' is the nonchiral SC state in which the pairing function is approximately described as $\Delta(\mathbf{k}) \sim \phi_a(\mathbf{k}) - \phi_b(\mathbf{k})$, while phases I, II, and III are the chiral SC states in which $\Delta(\mathbf{k}) \sim \phi_a(\mathbf{k}) + i\phi_b(\mathbf{k})$. The vortex lattice structures in phases I (I'), II, and III are illustrated on top of the phase diagram.

First, we show the phase diagram for $\nu = 0.15$ in Fig. 7. Indeed, the vortex lattice structural transition occurs, and three phases, I (I'), II, and III, appear. Although the square or rectangular lattice is formed in the absence of the nematicity (see Fig. 4), a centered rectangular lattice is stabilized in phases I and I' near T_c . This is intuitively understood as follows. Although a finite chirality is slightly induced by the gradient mixing, the order parameter is approximately nonchiral, $(\eta_1, \eta_2) \propto (1, -i)$, in the high-temperature region near T_c . Thus, an elongated triangular vortex lattice is stabilized as in single-component superconductors. Note that the elongated triangular lattice is equivalent to the centered rectangular

lattice.

We would like to stress that the symmetry-breaking term significantly affects the vortex lattice structure even below the C-NC crossover temperature. We define the C-NC crossover line dividing phases I and I' using the variational parameters as $|C_-| = 0.7|C_+|$. We see that the centered rectangular lattice (which equals the elongated triangular lattice) is stabilized well below the C-NC crossover temperature. Thus, the vortex lattice structure in chiral superconductors is sensitive to the nematic order. This is because of the small stiffness of Abrikosov vortex lattice and the large coupling of nematicity and chirality in superconductors.

The vortex lattice structure in phase II is interpreted to be a distorted rectangular lattice. A nematicity gives rise to a stress along the $[110]$ axis, and therefore, the rectangular lattice is deformed to an oblique lattice ($\rho \neq 0, 1/2$) in phase II. In particular, a marked effect of nematicity appears near the second-order phase transition to phase I, as we show the temperature dependence of variational parameters in Fig. 8. The structural parameter is $\rho = 1/2$ in phase I (centered rectangular lattice) and decreases to $\rho = 0$ (rectangular lattice) with decreasing temperature in phase II. At the same time the angle of the primitive vector θ rotates from $\theta = \pi/4$ to $\theta \sim 0$. The second-order transition from phase I to phase II is accompanied by the spontaneous violation of the reflection symmetry along the $[110]$ axis. Thus, we see marked signatures of nematic order in the vortex lattice structure in the low-temperature phase II. We show typical vortex lattice structures in phases I and II in Fig. 9(a) and 9(b), respectively.

The square vortex lattice is deformed to the centered rectangular lattice in the high-field phase III owing to the symmetry-breaking term. Then, $\theta_L \neq \pi/2$; however, the deformation is negligible, as shown in Fig. 10. The structural phase transition between phase II and phase III is characterized by the increase in b/a , as it occurs in the absence of nematicity (see Fig. 5).

Although the phase transition between phases II and III is specific for the parameter $\nu = 0.15$, the vortex lattice structural transition between phases I and II is ubiquitous as it is induced by the C-NC crossover. Indeed, the latter occurs for a wide range of the anisotropy parameter ν . For instance, we show the phase diagram at $\nu = 0.3$ (Fig. 11). It is shown that the vortex lattice structural transition is induced by the C-NC crossover. The centered rectangular lattice is stabilized in the high-temperature phases I and I', while the oblique lattice is stabilized in the low-temperature phase II, similar to the case of $\nu = 0.15$. Although the centered rectangular lattice is stable in the absence of the nematicity for $\nu = 0.3$ (see Fig. 6), it is deformed to the oblique lattice because the primitive vectors \mathbf{a}_1 and \mathbf{a}_2 are not parallel to the stress along the $[110]$ axis. The orientation of the vortex lattice is significantly rotated from $\theta = \pi/4$ to $\theta \sim 0$ by decreasing the temperature in phase II. Interestingly, a structural parameter ρ shows a marked change from

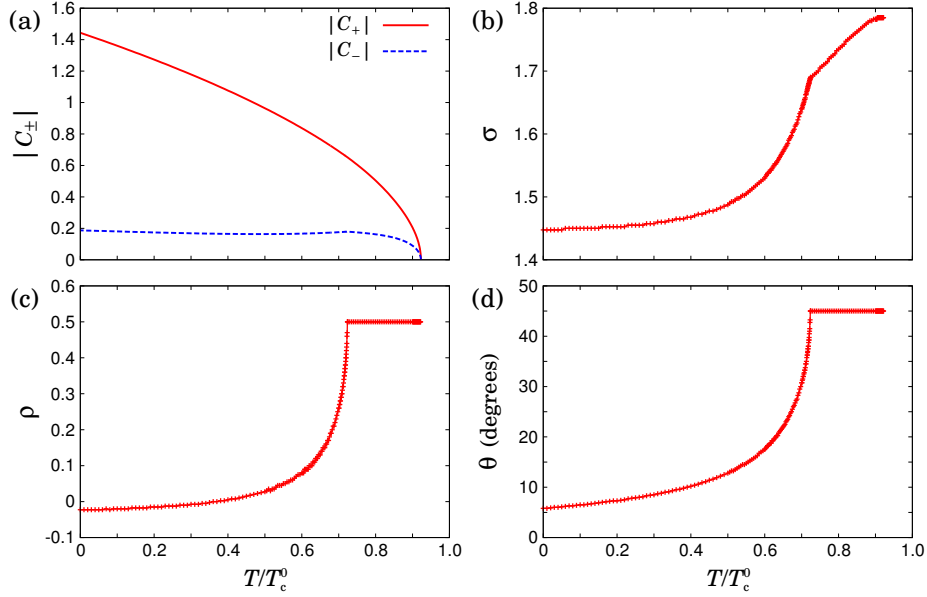


FIG. 8. (Color online) Temperature dependence of (a) order parameters $|C_{\pm}|$ and structural parameters (b) σ , (c) ρ , and (d) θ at $H/H_{c2}(0) = 0.1$ for $(\nu, g) = (0.15, 0.05)$.

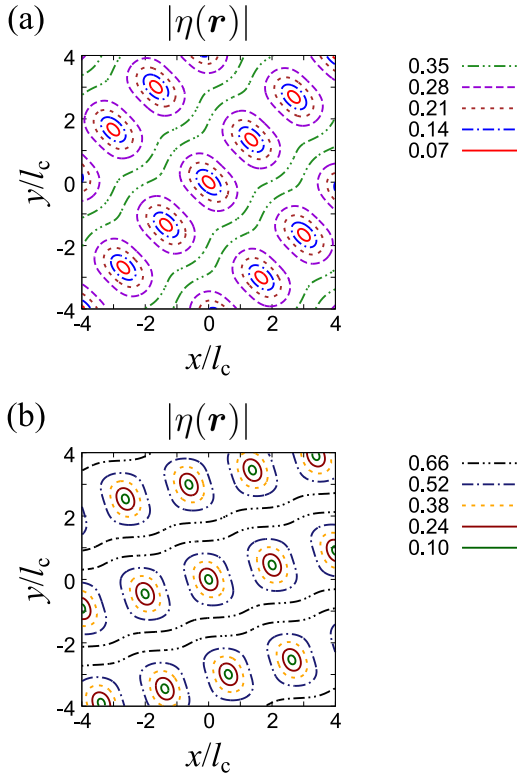


FIG. 9. (Color online) Vortex lattice structures (a) in phase I and (b) in phase II for $(\nu, g) = (0.15, 0.05)$. We choose $T/T_c^0 = 0.8$ and $H/H_{c2}(0) = 0.1$ in (a) and $T/T_c^0 = 0.5$ and $H/H_{c2}(0) = 0.1$ in (b). We show the amplitude of the order parameter $|\eta(\mathbf{r})|$, which is obtained by $|\eta(\mathbf{r})|^2 = |\eta_1(\mathbf{r})|^2 + |\eta_2(\mathbf{r})|^2$.

$\rho = 0.5$ to $\rho \sim -0.4$ at the same time.

Our results for $\nu = 0.15$ and $\nu = 0.3$ imply that the angle of a primitive vector from the x axis θ plays an important role in the vortex lattice structural transition. The x axis is no longer a principal axis of the electronic state for $g \neq 0$. Because the primitive vector should be parallel to the principal axis in the nonchiral state, we obtain $\theta = \pm\pi/4$ above the C-NC crossover temperature. The vortex lattice structural transition is induced by the C-NC crossover when we obtain $\theta \sim 0$ in the chiral state. As shown in Fig. 3, this condition is satisfied for $\nu > 0.00114$ since the vortex lattice structure in the chiral state is little affected by the symmetry-breaking term. As expected from this consideration, the vortex lattice structural transition between phases I and II disappears when $\nu < -0.00114$. Then, $\theta = \pm\pi/4$ in the whole SC state, as we will show in the next section.

C. Vortex lattice in the nematic state ($\nu < 0$)

As expected from the above discussions, Fig. 12 shows the H - T phase diagram without any structural phase transition for $\nu = -0.15$ and $\nu = -0.3$. The C-NC crossover occurs, as indicated by the dotted lines. However, the vortex lattice structural transition does not occur because the stress due to the nematicity is applied parallel to a primitive vector of the vortex lattice ($\theta = \pi/4$). The rectangular lattice and centered rectangular lattice are stabilized in the whole SC state for $\nu = -0.15$ and for $\nu = -0.3$, respectively. The effect of nematicity is only the increase in the parameter σ . The sign of the coupling constant g determines the orienta-

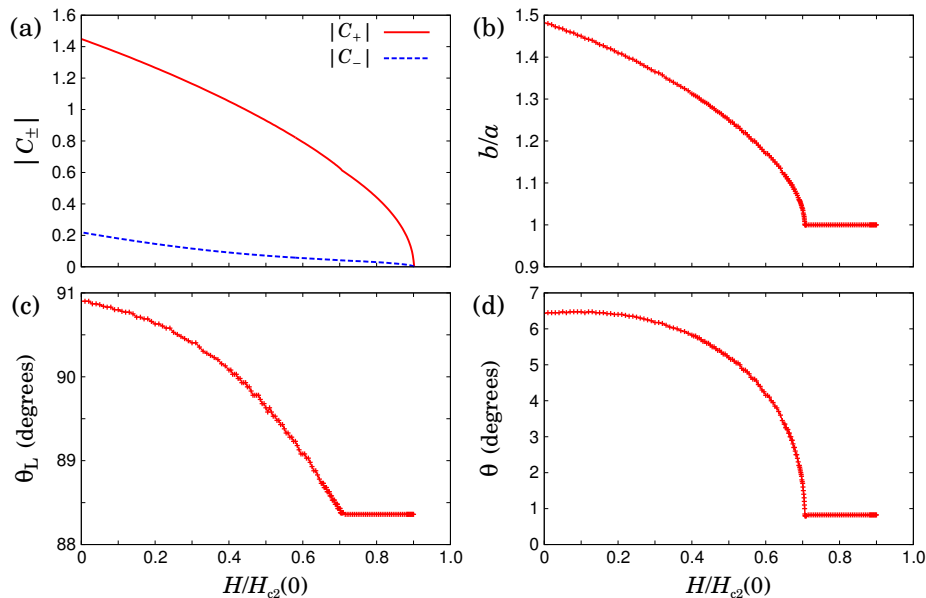


FIG. 10. (Color online) Magnetic field dependence of (a) order parameters $|C_{\pm}|$ and structural parameters (b) b/a , (c) θ_L , and (d) θ at $T/T_c^0 = 0.1$ for $(\nu, g) = (0.15, 0.05)$. We show b/a and θ_L instead of σ and ρ .

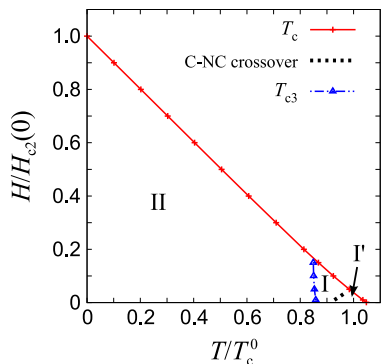


FIG. 11. (Color online) Phase diagram for $(\nu, g) = (0.3, 0.05)$. The order parameter and vortex lattice structures in phases I, I', and II are similar to those in Fig. 7.

tion of the elongated vortex lattice. When we choose $\sigma \geq 1$ for $\rho = 0$ and $\sigma \geq 1/2$ for $\rho = 1/2$, the orientation is $\theta = \pi/4$ for $g > 0$, while $\theta = -\pi/4$ for $g < 0$. For $\nu = -0.15$, the square-rectangular structural transition occurs at $g = 0$, but it is smeared by the external nematic order. The square lattice is deformed to the rectangular lattice owing to nematic order.

IV. SUMMARY AND DISCUSSION

In this paper we studied chiral SC states coexisting with a nematic order. The phase diagram of the order parameter and vortex lattice structure has been clarified on the basis of the two-component GL model. It is shown

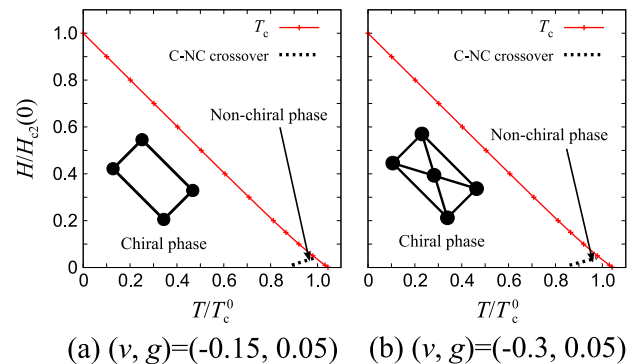


FIG. 12. (Color online) Phase diagram for $\nu < 0$. (a) The rectangular lattice ($\rho = 0, \theta = \pi/4$) is stable in the whole region of the SC state for $(\nu, g) = (-0.15, 0.05)$, while (b) the centered rectangular lattice is stable for $(\nu, g) = (-0.3, 0.05)$.

that the vortex lattice structure is sensitive to the chirality in Cooper pairs as well as to the nematicity in the electronic state. Because the chirality and nematicity cooperate in a nontrivial way, various vortex lattice structures are stabilized. In particular, the structural phase transition occurs in the vortex lattice when the nematicity is along the $[110]$ axis and the anisotropy parameter is positive $\nu > 0$, or when the nematicity is along the $[100]$ axis and $\nu < 0$ ³⁷. Otherwise, the vortex lattice structural transition is not induced by the nematic order, although the structural parameters are affected by the C-NC crossover in the pairing function. The structural phase transition and structural change discussed in this work are distinguished from those due to the anisotropy in the Fermi surface and SC gap^{40,41}, gra-

dent mixing in several irreducible representations⁴², and the Pauli depairing effect^{43,44}. The former occurs in the low-magnetic-field region near T_c , although the latter appears in the high-magnetic-field region.

Finally, we discuss the vortex state in the chiral superconductors on the basis of our results. Our study has been mainly focused on a heavy-fermion superconductor URu₂Si₂¹⁸ in which nematic order has attracted much attention recently. The nematicity observed by several experiments^{19–22} is along the [110]-direction. When we assume that two heavy Fermi surfaces around the M point cause the superconductivity, the anisotropy parameter is estimated to be $\nu = 0.41$ ⁴⁵ on the basis of the band structure calculation⁴⁶ and the Shubnikov-de Haas measurement⁴⁷. Thus, it is reasonable to assume a positive ν , although the anisotropy parameter should be affected by the multiband structure. According to our results, it is expected that the structural phase transition will occur in the vortex state under the c -axis magnetic field. If it were observed by a small-angle neutron scattering (SANS) measurement⁴⁸, for instance, clear evidence for both nematic order and chiral superconductivity would be obtained.

SANS measurements reported a square vortex lattice in Sr₂RuO₄⁴⁹. The orientation is $\theta = \pi/4$, implying a small negative parameter $\nu < 0$, and therefore, a nematicity along the [100] axis may induce the vortex lattice structural transition. Then, the symmetry-breaking term deforms the square lattice to the centered rectangular lattice at low temperatures. On the other hand, the nonchiral SC state with another centered rectangular vortex lattice is stabilized near T_c . The two vortex lattices have the same symmetry; however, the structural parameters are quite different. For instance, our calculation for $\nu = -0.05$ and $g = 0.01$ shows that the structural parameter is $2\sigma \sim 1.1$ in the chiral SC state but $2\sigma \sim 3.0$ in the nonchiral SC state. Thus, the vortex lattice structural change accompanying the C-NC crossover may be caused by the uniaxial pressure along the [100] axis. Interestingly, a significant enhancement of the transition temperature due to the uniaxial pressure has been observed³⁰. However, we should discuss the spin degree of freedom in Cooper pairs because Sr₂RuO₄ is considered to be a spin-triplet superconductor^{1,2}. When the spin-orbit coupling in Cooper pairs is small enough to allow the rotation of the d vector, a helical SC state, such as $\mathbf{d} = p_x\hat{x} - p_y\hat{y}$, is stabilized in the c -axis magnetic field⁵⁰. This state is beyond the scope of this paper, but it is expected that the nematicity affects the vortex lattice structure through the crossover in the pairing function. For instance, the nematicity along the [100] axis

stabilizes a planar state $\mathbf{d} = p_x\hat{x}$ or $\mathbf{d} = p_y\hat{y}$ near T_c , while the helical state is robust at low temperatures.

The symmetry of the pairing state in UPt₃ is controversial despite intensive studies for more than three decades. A recent polar Kerr rotation measurement found a spontaneous time-reversal symmetry-breaking, which implies a chiral SC state $\mathbf{d}(\mathbf{k}) = [\phi_a(\mathbf{k}) \pm i\phi_b(\mathbf{k})]\hat{c}$ ¹⁰, consistent with the suppression of the upper critical field along the c axis²⁷. On the other hand, NMR data indicate a rotation of the d vector⁵¹ and implies a helical SC state, such as $\mathbf{d}(\mathbf{k}) = \phi_a(\mathbf{k})\hat{b} + \phi_b(\mathbf{k})\hat{c}$. As for the orbital symmetry, the E_{2u} and E_{1g} representations have been considered as predominant candidates^{27,28}. On the other hand, a recent thermal conductivity measurement is consistent with the E_{1u} orbital symmetry with a hybrid nodal structure³⁶. Among these SC states, the chiral E_{1u} state and chiral E_{1g} state are described by the extended Agterberg model, and then, the square anisotropy parameter has to be zero, $\nu = 0$, owing to the hexagonal symmetry in the crystal lattice. Unfortunately, this model seems to be incompatible with several experimental results. First, the SC double transition is smeared in the c -axis magnetic field, although it has been observed in experiments^{25–28}. Second, the vortex lattice structure significantly changes through the C-NC crossover, although only a realignment without any structural deformation has been observed by a SANS measurement⁵². In order to avoid these discrepancies, we have to assume parameters in the GL model without relying on the extended Agterberg model. The parameters allowed by symmetry³⁸, $\kappa_2 \simeq \kappa_1$ and $\kappa_3 = \kappa_4 \simeq 0$, may be compatible with those experiments and may be consistent with the nearly isotropic upper critical field in the basal plane³⁶. Although these parameters are naturally obtained by the weak-coupling theory for the E_{2u} state²⁷, a fine-tuning of pairing functions and Fermi surfaces is required for the chiral E_{1u} and E_{1g} states.

ACKNOWLEDGMENTS

The authors are grateful to D. F. Agterberg, D. Aoki, H. Harima, T. Kita, T. Shibauchi, and M. Yokoyama for fruitful discussions. S. T. is supported by a Japan Society for the Promotion of Science (JSPS) Research Fellowships for Young Scientists. This work was supported by Grants-in-Aid for Scientific Research (KAKENHI Grants No. 25103711 and No. 24740230) from Ministry of Education, Culture, Sports, Science and Technology (MEXT) of Japan.

*

¹ A. P. Mackenzie and Y. Maeno, Rev. Mod. Phys. **75**, 657 (2003).

² Y. Maeno, S. Kittaka, T. Nomura, S. Yonezawa, and K.

Ishida, J. Phys. Soc. Jpn. **81**, 011009 (2012).

³ Y. Kasahara, T. Iwasawa, H. Shishido, T. Shibauchi, K. Behnia, Y. Haga, T. D. Matsuda, Y. Onuki, M. Sigrist, and Y. Matsuda, Phys. Rev. Lett. **99**, 116402 (2007).

- ⁴ K. Yano, T. Sakakibara, T. Tayama, M. Yokoyama, H. Amitsuka, Y. Homma, P. Miranović, M. Ichioka, Y. Tsutsumi, and K. Machida, *Phys. Rev. Lett.* **100**, 017004 (2008).
- ⁵ I. Kawasaki, I. Watanabe, A. Hillier, and D. Aoki, *J. Phys. Soc. Jpn.* **83**, 094720 (2014).
- ⁶ E. R. Schemm, R. E. Baumbach, P. H. Tobash, F. Ronning, E. D. Bauer, and A. Kapitulnik, arXiv:1410.1479.
- ⁷ T. Yamashita, Y. Shimoyama, Y. Haga, T. D. Matsuda, E. Yamamoto, Y. Onuki, H. Sumiyoshi, S. Fujimoto, A. Levchenko, T. Shibauchi, and Y. Matsuda, *Nat. Phys.* **11**, 17 (2014).
- ⁸ G. M. Luke, Y. Fudamoto, K. M. Kojima, M. I. Larkin, J. Merrin, B. Nachumi, Y. J. Uemura, Y. Maeno, Z. Q. Mao, Y. Mori, H. Nakamura, and M. Sgrist, *Nature (London)* **394**, 558 (1998).
- ⁹ J. Xia, Y. Maeno, P. T. Beyersdorf, M. M. Fejer, and A. Kapitulnik, *Phys. Rev. Lett.* **97**, 167002 (2006).
- ¹⁰ E. R. Schemm, W. J. Gannon, C. M. Wishne, W. P. Halperin, and A. Kapitulnik, *Science* **345**, 190 (2014).
- ¹¹ E. Fradkin, S. A. Kivelson, M. J. Lawler, J. P. Eisenstein, and A. P. Mackenzie, *Annu. Rev. Condens. Matter Phys.* **1**, 153 (2010).
- ¹² S. A. Kivelson, I. P. Bindloss, E. Fradkin, V. Oganesyan, J. M. Tranquada, A. Kapitulnik, and C. Howald, *Rev. Mod. Phys.* **75**, 1201 (2003).
- ¹³ A. P. Mackenzie, J. A. N. Bruin, R. A. Borzi, A. W. Rost, and S. A. Grigera, *Phys. C (Amsterdam, Neth.)* **481**, 207 (2012).
- ¹⁴ R. M. Fernandes, L. H. VanBebber, S. Bhattacharya, P. Chandra, V. Keppens, D. Mandrus, M. A. McGuire, B. C. Sales, A. S. Sefat, and J. Schmalian, *Phys. Rev. Lett.* **105**, 157003 (2010).
- ¹⁵ T. Goto, R. Kurihara, K. Araki, K. Mitsumoto, M. Akatsu, Y. Nemoto, S. Tatematsu, and M. Sato, *J. Phys. Soc. Jpn.* **80**, 073702 (2011).
- ¹⁶ H. Kontani and S. Onari, *Phys. Rev. Lett.* **104**, 157001 (2010).
- ¹⁷ Y. Yanagi, Y. Yamakawa, N. Adachi, and Y. Ono, *J. Phys. Soc. Jpn.* **79**, 123707 (2010).
- ¹⁸ J. A. Mydosh and P. M. Oppeneer, *Rev. Mod. Phys.* **83**, 1301 (2011).
- ¹⁹ R. Okazaki, T. Shibauchi, H. J. Shi, Y. Haga, T. D. Matsuda, E. Yamamoto, Y. Onuki, H. Ikeda, and Y. Matsuda, *Science* **331**, 439 (2011).
- ²⁰ S. Tonegawa, K. Hashimoto, K. Ikada, Y.-H. Lin, H. Shishido, Y. Haga, T. D. Matsuda, E. Yamamoto, Y. Onuki, H. Ikeda, Y. Matsuda, and T. Shibauchi, *Phys. Rev. Lett.* **109**, 036401 (2012).
- ²¹ S. Kambe, Y. Tokunaga, H. Sakai, T. D. Matsuda, Y. Haga, Z. Fisk, and R. E. Walstedt, *Phys. Rev. Lett.* **110**, 246406 (2013).
- ²² S. Tonegawa, S. Kasahara, T. Fukuda, K. Sugimoto, N. Yasuda, Y. Tsuruhara, D. Watanabe, Y. Mizukami, Y. Haga, T. D. Matsuda, E. Yamamoto, Y. Onuki, H. Ikeda, Y. Matsuda, and T. Shibauchi, *Nat. Commun.* **5**, 4188 (2014).
- ²³ T. Mito, M. Hattori, G. Motoyama, Y. Sakai, T. Koyama, K. Ueda, T. Kohara, M. Yokoyama, and H. Amitsuka, *J. Phys. Soc. Jpn.* **82**, 123704 (2013).
- ²⁴ R. Okazaki, M. Shimozawa, H. Shishido, M. Konczykowski, Y. Haga, T. D. Matsuda, E. Yamamoto, Y. Onuki, Y. Yanase, T. Shibauchi, and Y. Matsuda, *J. Phys. Soc. Jpn.* **79**, 084705 (2010).
- ²⁵ S. Adenwalla, S. W. Lin, Q. Z. Ran, Z. Zhao, J. B. Kettererson, J. A. Sauls, L. Taillefer, D. G. Hinks, M. Levy, and Bimal K. Sarma, *Phys. Rev. Lett.* **65**, 2298 (1990).
- ²⁶ S. M. Hayden, L. Taillefer, C. Vettier, and J. Flouquet, *Phys. Rev. B* **46**, 8675(R) (1992).
- ²⁷ J. A. Sauls, *Adv. Phys.* **43**, 113 (1994).
- ²⁸ R. Joynt and L. Taillefer, *Rev. Mod. Phys.* **74**, 235 (2002).
- ²⁹ G. Aeppli, E. Bucher, C. Broholm, J. K. Kjems, J. Baumann and J. Hufnagl, *Phys. Rev. Lett.* **60**, 615 (1988).
- ³⁰ C. W. Hicks, D. O. Brodsky, E. A. Yelland, A. S. Gibbs, J. A. N. Bruin, M. E. Barber, S. D. Edkins, K. Nishimura, S. Yonezawa, Y. Maeno, and A. P. Mackenzie, *Science*, **344**, 283 (2014).
- ³¹ D. F. Agterberg, *Phys. Rev. Lett.* **80**, 5184 (1998).
- ³² D. F. Agterberg, *Phys. Rev. B* **58**, 14484 (1998).
- ³³ T. Kita, *Phys. Rev. Lett.* **83**, 1846 (1999).
- ³⁴ M. Sgrist and K. Ueda, *Rev. Mod. Phys.* **63**, 239 (1991).
- ³⁵ M. Sgrist, D. Agterberg, A. Furusaki, C. Honerkamp, K. K. Ng, T. M. Rice and M. E. Zhitomirsky, *Phys. C (Amsterdam, Neth.)* **317–318**, 134 (1999).
- ³⁶ Y. Machida, A. Itoh, Y. So, K. Izawa, Y. Haga, E. Yamamoto, N. Kimura, Y. Onuki, Y. Tsutsumi, and K. Machida, *Phys. Rev. Lett.* **108**, 157002 (2012).
- ³⁷ The sign of ν in Eq. (2) is opposite to the definition in Refs.^{31,32}.
- ³⁸ This relation is satisfied within the extended Agterberg model. Generally, the hexagonal D_{6h} point group symmetry imposes relations $\beta_3 = 0$ and $\kappa_3 = \kappa_4 = (\kappa_1 - \kappa_2)/2^{27}$.
- ³⁹ I. A. Luk'yanchuk and M. E. Zhitomirsky, *Supercond. Rev.* **1**, 207 (1995).
- ⁴⁰ Y. De Wilde, M. Iavarone, U. Welp, V. Metlushko, A. E. Koshelev, I. Aranson, G. W. Crabtree, and P. C. Canfield, *Phys. Rev. Lett.* **78**, 4273 (1997).
- ⁴¹ N. Nakai, P. Miranovic, M. Ichioka, and K. Machida, *Phys. Rev. Lett.* **89**, 237004 (2002).
- ⁴² I. Affleck, M. Franz, and M. H. Sharifzadeh Amin, *Phys. Rev. B* **55**, R704 (1997).
- ⁴³ A. D. Bianchi, M. Kenzelmann, L. DeBeer-Schmitt, J. S. White, E. M. Forgan, J. Mesot, M. Zolliker, J. Kohlbrecher, R. Movshovich, E. D. Bauer, J. L. Sarrao, Z. Fisk, C. Petrovic, and M. R. Eskildsen, *Science*, **319**, 177 (2008).
- ⁴⁴ N. Hiasa and R. Ikeda, *Phys. Rev. Lett.* **101**, 027001 (2008).
- ⁴⁵ S. Takamatsu, H. Harima, D. Aoki, and Y. Yanase (unpublished).
- ⁴⁶ H. Harima (private communication).
- ⁴⁷ D. Aoki, G. Knebel, I. Sheikin, E. Hassinger, L. Malone, T. D. Matsuda, and J. Flouquet, *J. Phys. Soc. Jpn.* **81**, 074715 (2012).
- ⁴⁸ M. R. Eskildsen, *Front. Phys.* **6**, 398 (2011).
- ⁴⁹ T. M. Riseman, P. G. Kealy, E. M. Forgan, A. P. Mackenzie, L. M. Galvin, A. W. Tyler, S. L. Lee, C. Ager, D. McK. Paul, C. M. Aegerter, R. Cubitt, Z. Q. Mao, T. Akima, and Y. Maeno, *Nature (London)* **396**, 242 (1998); **404**, 629 (2000).
- ⁵⁰ S. Takamatsu and Y. Yanase, *J. Phys. Soc. Jpn.* **82**, 063706 (2013).
- ⁵¹ H. Tou, Y. Kitaoka, K. Ishida, K. Asayama, N. Kimura, Y. Onuki, E. Yamamoto, Y. Haga, and K. Maezawa, *Phys. Rev. Lett.* **80**, 3129 (1998).
- ⁵² A. Huxley, P. Rodière, D. McK. Paul, N. van Dijk, R. Cubitt, and J. Flouquet, *Nature (London)* **406**, 160 (2000).